

Full-Color Electrophoretic Display Using Charged Colloidal Arrays of Core–Shell Microspheres with Enhanced Color Tunability in Non-Polar Medium

Eunseon Park, Seungju Lee, Hyunjung Lee, and Wonmok Lee*

In this study, core–shell microspheres of poly(methylmethacrylate) (PMMA) and poly(*t*-butylmethacrylate) (PtBMA) are synthesized and dispersed in a non-polar medium exhibiting a structural color in the visible range. The charge stabilization of the PMMA–PtBMA microsphere is achieved because of preferential adsorption of the charged inverse micelles of aerosol-OT (AOT) on the microsphere surface. While the PtBMA shell enables the dispersion of the microspheres in isoparaffinic fluid, the PMMA core provides an enhanced refractive index contrast with the medium. In comparison to PtBMA-only microsphere, incorporation of PMMA core not only increases the average refractive index but also increases the surface charge density of the microsphere, which is attributed to strong attraction between the inverse micelles and the microsphere. The optimized crystalline colloidal array (CCA) of the PMMA–PtBMA microsphere shows stronger structural colors than those of the PtBMA-only spheres because of an enhanced index contrast with the liquid medium, and an improved color tunability is also achieved. A CCA exhibits approximately 50% light transmittance, demonstrating a semi-transparent display. The repeated voltage biases proved that a CCA has excellent stability. Finally, a low-angular dependency of the PMMA–PtBMA CCA is confirmed, which is an advantageous feature as an electrophoretic display.

1. Introduction


A photonic crystal (PC) can modulate light propagation due to the unique photonic bandgap or stopband properties originating from the interaction of light with the long-range ordered PC structure. Previous studies demonstrate a variety of fabrication methods for PCs. Among them, self-assembly from soft materials, such as artificial opals, liquid crystals (LCs), and block copolymers, is advantageous because of low processing

cost and efficient color tunability. Particularly, electrically tunable PCs have gained significant attention as promising candidates for full-color reflective displays.^[1] Depending on the operating principles, electrically tunable PCs can be categorized into four different types. The first type is based on an electrochemical process in which a redox reaction of the active material near the electrode modulates the PC structure.^[2] Ozin and coworkers demonstrate a colloidal PC containing embedded polyferrocenylsilane (PFS) in the interstitial spaces that undergoes an oxidation reaction by voltage bias. Because of charge accumulation, the oxidized form of the PFS induces swelling of the PC, consequently shifting the photonic stopband to a longer wavelength.^[2b] The oxidation state of the PFS is reversible by negative biasing, and various polymers that are capable of reversible redox reactions to altering the dimension of PCs (besides PFS) have been investigated.^[2a,c] The second type is based on electric-field responsive LC.^[3] In a crystalline phase, LC

becomes birefringent material that possesses different refractive indices depending on the direction and polarization of the incident light.^[4] This anisotropic optical property of LC enables the electrical tuning of transmittance or color. LC has been successfully applied to the color tuning of PCs. Recently, LC-containing PCs that apply nematic LCs and opaline PCs have been reported.^[3] For instance, a polymeric inverse opal was infiltrated with 4-pentyl-4'-cyanobiphenyl (5CB) as the LC, and high voltage ($6 \text{ V } \mu\text{m}^{-1}$) was applied for 2 ms to obtain a 35 nm blue shift in the reflection peak.^[3a] To improve the repeatability of color tuning, Kubo et al. reported photo-tunable and electric-tunable LCs by mixing 5CB with an azobenzene moiety. After infiltrating the LC mixture in an inverse opal structure, the PC structure exhibited low transmittance due to light scattering, whereas the application of an electric field altered the orientation of the LC molecules to increase transmittance by refractive index modulation.^[3b] In the third type of electrically tunable PC, the electric field is utilized as a second stimulus, inducing a process that acts as a primary stimulus for the desired property changes.^[5] For example, Xia et al. demonstrated electric tuning of photonic stopbands by straining a polymeric opal within two carbon-silicone composite electrodes

E. Park, S. Lee, W. Lee
Department of Chemistry
Sejong University
98 Gunja-dong, Gwangjin-gu, Seoul 143-747, Korea
E-mail: wonmoklee@sejong.ac.kr

H. Lee
School of Advanced Materials Engineering
Kookmin University
861-1 Jeongneung-dong, Seoul 136-702, Korea

 The ORCID identification number(s) for the author(s) of this article can be found under <https://doi.org/10.1002/adom.202100833>.

DOI: 10.1002/adom.202100833

that exert Maxwell stress.^[5b] Upon voltage bias, the opal film compresses, resulting in a structural color change by variation among interparticle distances. Another indirect method is reported by Jiang et al., in which a thermoresponsive LC-based inverse opal is expanded via Joule heating upon the application of an electric field, resulting in a color change.^[6] The last and most preferred type of electrically tunable PC is based on the electrophoretic movement of the crystalline colloidal array (CCA).^[7] The origin of the electrophoretic display (EPD) is e-ink technology in which the liquid dispersions of negatively charged white TiO_2 particles and positively charged black carbon nanoparticles are placed between two transparent electrodes.^[8] Voltage bias induces the electrophoretic migrations of black and white particles in opposite directions, generating black and white contrast.^[8a] Although e-ink initiated the ultra-low-power e-book market, the basic principle only allows a monochromatic display. Unlike conventional e-ink technology, electrophoretic migration of charged CCAs enables full RGB color tuning in one pixel. Thus, various CCA systems have recently been extensively studied. Shim et al. demonstrate a full-color EPD using a polymeric CCA synthesized by emulsion polymerization.^[7b] CCAs from inorganic microspheres (μ -spheres) such as ZnS/SiO_2 , $\text{TiO}_2/\text{SiO}_2$, and $\text{Fe}_3\text{O}_4/\text{SiO}_2$ are also reported.^[7a,c,e,i] If a CCA is assembled in a face-centered cubic (FCC) structure without defect, the reflective color will have angular dependence as predicted by Bragg diffraction, as shown in Figure 1a. Depending on the size distribution and

the stability of the dispersion, however, the CCA can have a quasi-amorphous structure as shown in Figure 1b. In this structure, long-range ordering is weakened and angle dependence becomes less serious.^[7a,g]

In the majority of the studies on CCA-based EPDs, particles are dispersed in polar media such as water or propylene carbonate to ensure surface charges on the μ -spheres. However, a polar medium with a high dielectric constant is disadvantageous for stability. Hsu et al. showed that the charge stabilizations of polymeric μ -spheres in a non-polar medium are adsorbed on μ -spheres when aided by inverse micelles of di(2-ethylhexyl) sulfosuccinate (AOT).^[9] Ge et al. reported an assembly of magnetically tunable $\text{Fe}_3\text{O}_4/\text{SiO}_2$ μ -spheres in dichlorobenzene using AOT.^[10] In our group's previous report, a CCA from poly(*t*-butylmethacrylate) (PtBMA) μ -spheres was fabricated in isoparaffinic fluid in the presence of AOT, successfully demonstrating an electrically tunable full-color display (Figure S1, Supporting Information).^[7i]

Despite multiple advantageous features such as small operating current and full RGB color tunability, the CCA from PtBMA μ -spheres exhibits a relatively low index contrast in non-polar liquid because of the inherently low refractive index of PtBMA, and the blue-shifted color at high voltage (>4 V) was particularly faint.^[7i] In this study, a full-color EPD using poly(methylmethacrylate) (PMMA)–PtBMA core-shell μ -spheres with enhanced index contrast and surface charge density is examined. Rigorous analyses on electrically tunable

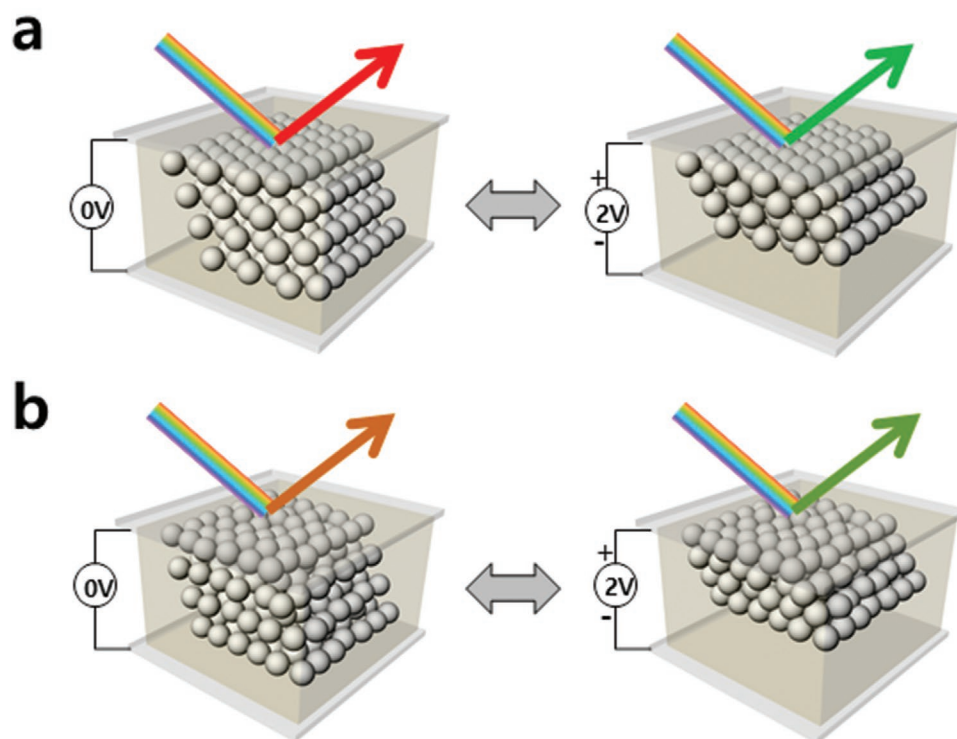


Figure 1. Schematic illustrations of full-color EPD devices consisting of the ordered arrays of charged μ -spheres dispersed in liquid media between two transparent electrodes. Bragg diffractions from close-packed layers parallel to the electrode surface are responsible for colors that can be tuned using voltage bias. The arrangements of μ -spheres can be either a) CCA or b) QACA structures.

core-shell CCAs (such as long-term stability, semi-transparency, and angular dependency) are performed.

2. Results and Discussion

In the previous investigation, it was discovered that the PtBMA μ -spheres were an optimized material for forming a good CCA in a mixture of IPG and HC oil in the presence of AOT inverse micelles.^[7] The PtBMA ($n = 1.46$) dispersed in a 1.7/1 (v/v) mixture of IPG/HC ($n = 1.39$) resulted in a small difference in refractive indices (Δn) of 0.07. To improve the index contrast, a PMMA ($n = 1.49$) core was introduced in this study, and the PtBMA shell was formed by the subsequent addition of a tBMA monomer to ensure the dispersity of the μ -spheres. As shown in Figure S2, Supporting Information, the μ -spheres were sampled before and after the addition of tBMA, and the increased diameter was evident in showing the formation of PtBMA shell. Without PtBMA shells, PMMA μ -spheres readily aggregated after centrifugation.^[7] Core-shell μ -spheres with four different diameters (190, 200, 210, and 220 nm) were prepared after purification, the PMMA-PtBMA μ -spheres were thoroughly dispersed in DI water, as shown in Figure 2a. After the liquid was replaced by IPG/HC, the μ -spheres formed agglomerates at the bottom of the vial due to the decreased surface charge from the non-polar liquid, as shown in Figure 2a.

In a liquid with a dielectric constant as low as 2.0, the double-layer capacitance (C^d) of the particle surface is decreased by 40 times compared with that of water, resulting in approximately 40 times smaller surface charge density.^[11] The low surface charge of the μ -spheres in a non-polar liquid is overcome by introducing charged inverse micelles using AOT. As the chemical structure shows in Figure 2b, AOT is an ionic amphiphile. It is known to form inverse micelles in non-polar liquid over critical micellar concentration, as shown in Figure 2c.^[12] Because of its polar nature, the addition of AOT in IPG/HC increases the dielectric constants (ϵ) of the liquid medium, as shown in Table 1.^[13]

The collision of neutral micelles produces a pair of oppositely charged micelles. As is demonstrated in Figure 2c, the preferential adsorption of anionic inverse micelles on the surface of polymeric μ -spheres enables the charge stabilization of the μ -spheres in a non-polar medium.^[14] The development of surface charge on the μ -spheres provides the formation of a stable colloidal dispersion as shown in Figure 2a.^[9,14,15]

In Figure 2d, the zeta potentials of the PtBMA μ -spheres and PMMA-PtBMA core-shell μ -spheres with similar diameters (200 nm) that were respectively dispersed in IPG/HC/AOT were measured with varying concentrations of AOT. Both of the μ -sphere systems exhibited the maximum surface potentials at approximately the 100–150 mM AOT concentration range. The results demonstrate that as AOT concentration increases,

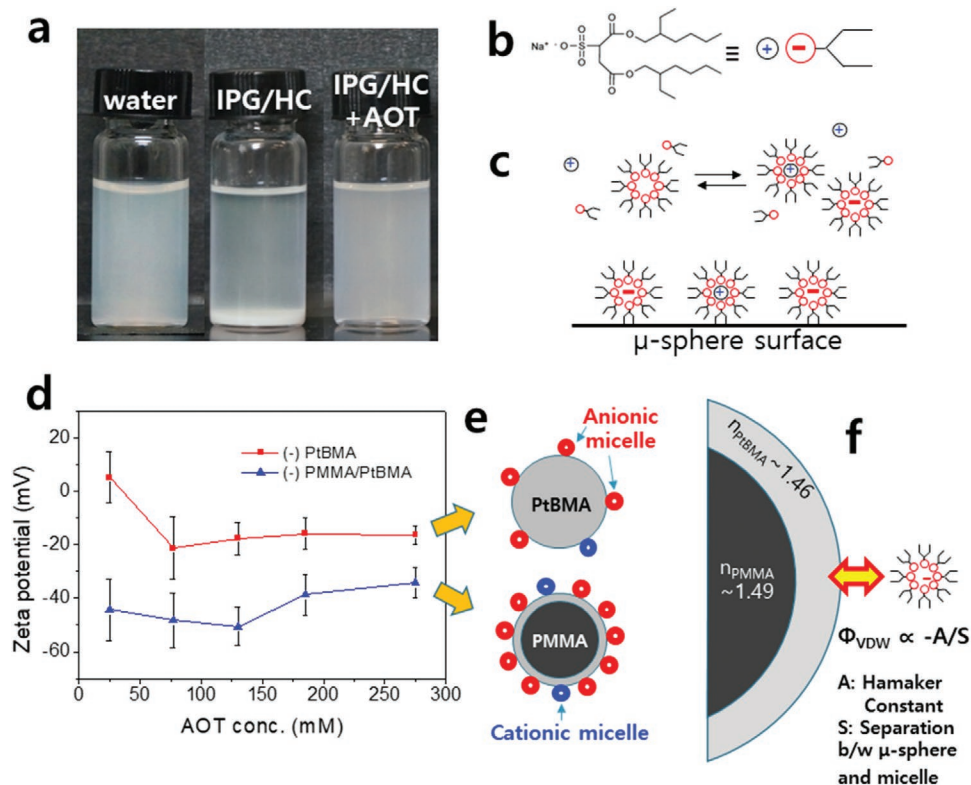


Figure 2. a) Colloidal dispersions of PMMA-PtBMA core-shell μ -spheres in water, IPG/HC, and IPG/HC with AOT. b) Molecular structure and schematic representation of AOT and c) formation of AOT inverse micelles and adsorption on the μ -sphere surface. d) Zeta potential (ζ) measurements of the colloidal dispersions of 200-nm-sized PtBMA μ -spheres and PMMA-PtBMA μ -spheres at different AOT concentrations. Schematic drawings of e) PMMA and PMMA-PtBMA μ -spheres with different densities of the adsorbed inverse micelles and f) VDW attraction of an AOT inverse micelle by a PMMA-PtBMA μ -sphere.

Table 1. Dielectric constants (ϵ) of IPG/HC with various AOT concentrations.

| AOT conc. [mM] | 25 | 75 | 130 | 185 | 275 |
|--------------------------------|------|------|------|------|------|
| $\epsilon_{\text{IPG/HC/AOT}}$ | 2.18 | 2.54 | 2.88 | 3.21 | 3.72 |

the surface charge decreases. This is due to the precedence of preferential adsorption of anionic micelles on particle surfaces followed by the adsorption of cationic micelles through the coulombic attraction between oppositely charged micelles [Figure 2e].

PMMA–PtBMA μ -spheres possess much higher surface potentials compared with those of PtBMA-only μ -spheres over the entire range of AOT concentrations, implying a greater surface charge density on the core–shell μ -spheres. This is schematically shown in Figure 2e. The higher surface potential of the core-shell μ -spheres was rationally attributed to the distinct index refractions of the two colloidal systems. Unlike the double layer charging mechanism of aqueous colloidal dispersions based on DLVO theory, particle charging in a non-polar medium requires adsorption of the charged micelles onto the particle surface. This primarily relies on van der Waals (VDW) attraction between the micelles and the particle, whereas the VDW interaction between two spherical particles with different radii is inversely proportional to the separation distance (S) where the Hamaker constant A is closely related to the polarization properties of the particles with radius r_1 and r_2 .^[16]

$$\Phi_{\text{VDW}} = -Ar_1r_2/6(r_1 + r_2)S \quad (1)$$

PMMA, having a higher index of refraction (1.49) than that of PtBMA (1.46), will exert a stronger attraction with AOT micelles since the relative refractive indices of the materials determine the attraction between particles.^[17] Although the PMMA core is hidden by the PtBMA shell, preventing direct contact between the high-index PMMA core and the AOT micelles, a relatively long-range VDW attraction can be effective by S^{-1} dependence, as shown in Figure 2f. Consequently, a strong VDW attraction between the high-index μ -sphere and the AOT micelles is responsible for the ζ as high as -50 mV in the non-polar medium.

To investigate the quality and electric tunability of the reflective color from the CCA of PMMA–PtBMA μ -spheres ($d = 200$ nm) in IPG/HC/AOT, a 1 cm^2 EPD cell containing colloidal dispersions of 40 wt.% was prepared with various AOT concentrations (Figure S3, Supporting Information). The size of the μ -sphere and its content in IPG/HC/AOT were optimized for the CCA to exhibit a full range of RGB color by electrical tuning as shown in Figures S3 and S4, Supporting Information. Figure 3a,b shows the changes in reflectance spectra and the corresponding colors under-voltage bias from 0 to 8 V upon a CCA with 130 mM AOT. With a voltage bias up to 4 V, color tunability ($d\lambda_{\text{max}}/dV$) was as high as 30 nm V^{-1} , whereas slight blue shifts in λ_{max} were observed at higher voltage biases. Figure 3b shows that full RGB color tuning was achieved by applying an 8 V bias. Two major noteworthy features of the CCA from

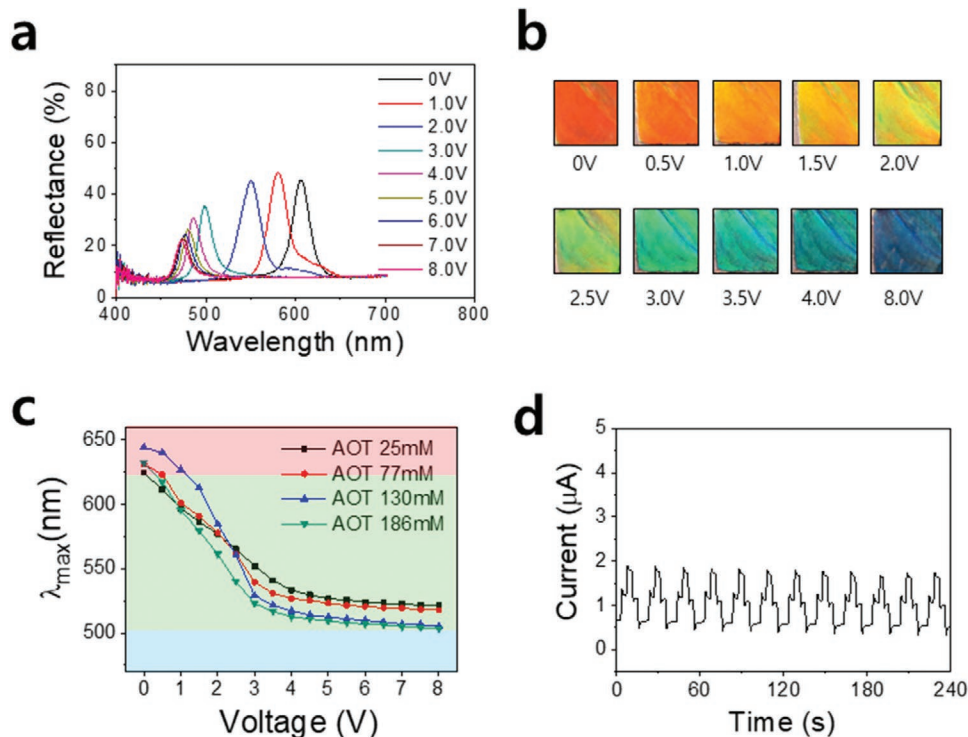


Figure 3. a) Electric tuning of the reflectance spectra obtained from the EPD cell containing the CCA of PMMA–PtBMA μ -spheres ($d = 200$ nm) in IPG/HC/AOT at 130 mM AOT content; b) the color changes of the display cell with voltage bias from 0 to 8 V, showing full RGB reflective colors; c) plots of λ_{max} versus voltage for the EPDs containing different AOT concentrations; and d) electric currents measured from a 1 cm^2 area EPD cell upon repeated voltage biases of 2–3 and 4–3 V. With a duration of 5 s for each voltage step, one cycle corresponds to 20 s.

PMMA–PtBMA core–shell μ -spheres are high color tunability and high color quality (particularly in the blue region).

Using the same PMMA–PtBMA μ -spheres at the same solid content, the CCAs were prepared with different AOT concentrations. As shown in the color tunability plots (λ_{\max} vs voltage) in Figure 3c, the highest tunability was achieved at the AOT concentration of 130 mM, which is in accordance with the ζ data in Figure 2d. There are 5 to 10% of differences of λ_{\max} values during E-tuning of 200nm-sized μ -sphere at the same AOT concentration (130 mM) in Figure 3a,c. Even though the same μ -sphere was used to prepare a CCA in IPG/HC at the same solid content and AOT concentration, there were slight batch-to-batch deviations in the reflection peak during E-tuning experiments. To examine the power consumption of the EPD device, the operating current was measured during the repeated voltage biasing on an EPD cell with a 1 cm² surface area. As shown in Figure 3d, repeated biases of 2–3 and 4–3 V (5 s duration at each voltage) produced an operating current of no more than 2 $\mu\text{A cm}^{-2}$. This operating current implies that the EPD has a very low power consumption. It has been proposed that even in EPDs, a small current can flow because of the charge injection at the electrode surface by a surfactant and a subsequent production of charged inverse micelles by replacement reaction.^[18] The observed current of 2 $\mu\text{A cm}^{-2}$ and its decreasing profile with time upon stepwise voltage bias coincides well with the transient current measurements from previous literature where Polyisobutylene succinimide was utilized as a surfactant and n-dodecane was utilized as a non-polar medium.^[18] Therefore, this study's results are explained by the generation of charged inverse micelles in a non-polar medium.^[18,19] When the CCA is infilled between flat substrates, the particular ordering is assumed to be FCC with the hexagonal close-packed plane parallel to the surface of the substrate.^[7b,20] It is generally accepted that the reflective color originates from the Bragg diffraction of the {111} planes, although a quasi-amorphous colloidal array (QACA)^[7a] or a mixture with CCA (depending on the nature of the colloidal dispersions) has been proposed.^[7i] Under the assumption of FCC-structured CCA formation for the colloidal system in this study, a modified Bragg equation using interparticle distance d , is described as Equation (2):^[7b]

Table 2. Inter-layer distance (D) at various AOT concentrations.

| AOT conc. [mM] | 25 | 77 | 130 | 186 |
|------------------|--------|--------|--------|--------|
| n_{eff} | 1.4506 | 1.4510 | 1.4514 | 1.4518 |
| D_{0V} [nm] | 263.6 | 266.3 | 271.8 | 266.7 |
| D_{8V} [nm] | 220.0 | 218.5 | 213.3 | 212.4 |
| ΔD [nm] | 43.6 | 47.8 | 58.5 | 54.3 |

$$\lambda_{\max} = \sqrt{8/3} \times n_{\text{eff}} \times d \quad (2)$$

where n_{eff} is calculated from the volume fraction (ϕ) and the indices of refraction for the μ -spheres ($n_{\mu\text{-sphere}}$) and the liquid medium ($n_{\text{interstice}}$) as follows:^[7b]

$$n_{\text{eff}} = (\phi_{\mu\text{-sphere}} \times n_{\mu\text{-sphere}}^2 + \phi_{\text{interstice}} \times n_{\text{interstice}}^2)^{0.5} \quad (3)$$

From scanning electron microscopy analysis, the average diameter of the PMMA-core particle and the core–shell μ -sphere were measured to be 182 and 200 nm, respectively. The volume ratio of PMMA and PtBMA was calculated as 3:1, and the $n_{\mu\text{-sphere}}$ of 1.484 was obtained. Under various AOT concentrations, $n_{\text{interstice}}$ was directly measured. From the measured μ -sphere content of 40 wt.% and the mass densities, volume fractions were also calculated. The resulting n_{eff} values are summarized in Table 2. Using the calculated d from the λ_{\max} under various AOT concentrations [as shown in Figure 3c], one can define an inter-layer distance (D) which corresponds to the spacing between two {111} crystal planes in CCA, and the inter-layer distances without or with voltage bias (D_{0V} and D_{8V}) were calculated. These results are shown in Table 2. The maximum difference between D_{0V} and D_{8V} (ΔD) was 58.5 nm and occurred at an AOT concentration of 130 mM. For better visualization of the interlayer distances, D_{0V} and D_{8V} versus AOT concentration data were plotted in Figure 4a.

Without an electric field, the trend in inter-layer distance (D_{0V}) with AOT concentration appeared to resemble that of the surface charge versus AOT plot in Figure 2d, implying that 130 mM AOT is the optimized concentration for both dilute and concentrated μ -sphere dispersions. Unlike D_{0V} , distance

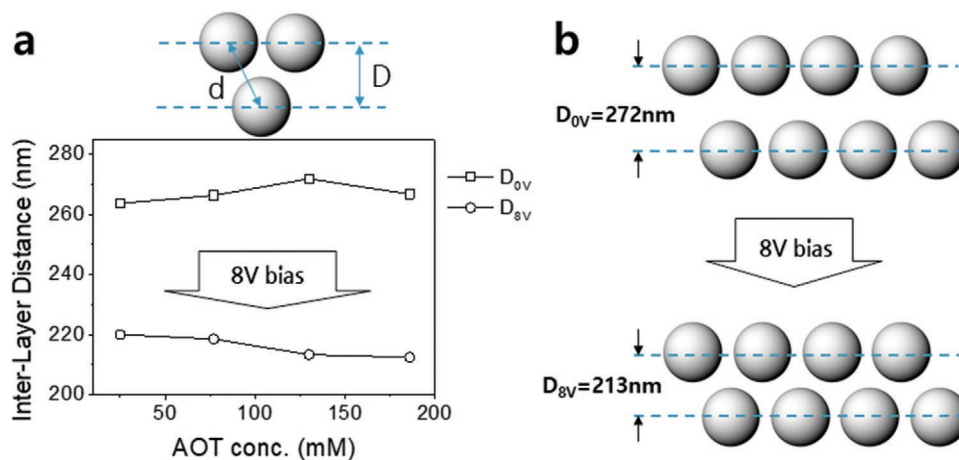


Figure 4. a) Plots of inter-layer distance as a function of AOT concentration with and without voltage bias. b) Schematic representation of D_{0V} and D_{8V} for an FCC-structured CCA under 130 mM AOT concentration.

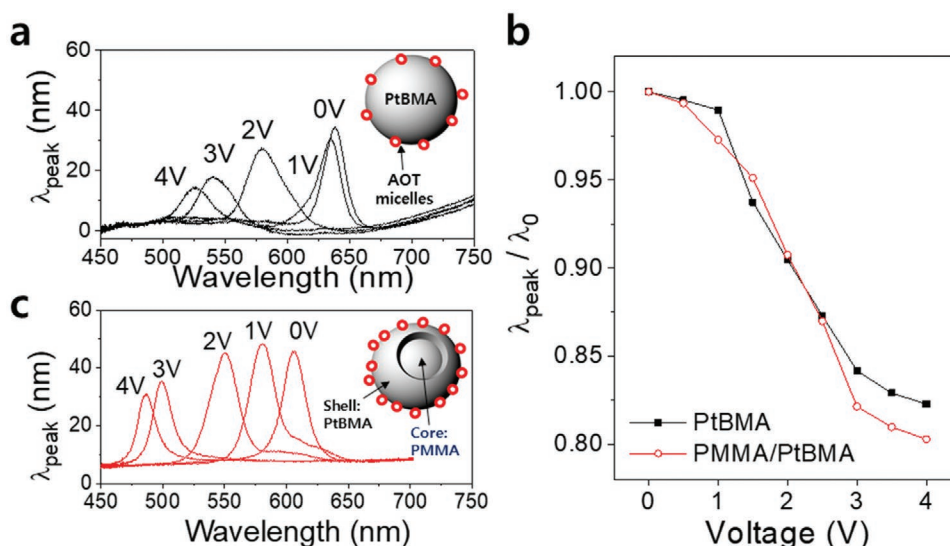


Figure 5. Comparison of reflectance spectra of the CCAs from a) the PtBMA-only μ -spheres, and b) the PMMA–PtBMA μ -spheres under-voltage bias from 0 to 4 V. c) Comparison of $\lambda_{\text{peak}}/\lambda_0$ versus voltage bias plots for the CCAs from 200-nm-sized PtBMA-only μ -spheres (black closed squares) and the same-sized PMMA–PtBMA core–shell μ -spheres (red open circles). A better electric tunability ($\Delta\lambda_{\text{peak}}/\Delta V$) for the core–shell CCA due to the higher surface charge on the high-index μ -spheres is observed.

D_{8V} showed an opposite (decreasing) trend with increasing AOT concentration: asymptotic behavior at AOT concentrations higher than 130 mM. This is attributed to the distinct charging behavior of the μ -sphere under an electric field.^[21] The trend is explained as follows: First, an increased AOT concentration from 25 to 186 mM allows the decreased double layer thickness (k^{-1}) to change from 53.0 to 24.3 nm (Figure S5, Supporting Information).^[22] Additionally, different ionic environments near the electrode affect μ -sphere charging. When the voltage is biased, the negatively charged μ -spheres migrate toward the anode surface, along which the unbound negatively charged micelles also migrate. Because of the enriched concentration profile of anionic micelles near the anode, the surface charge of a μ -sphere will be more negative, resulting in a higher susceptibility to the electric field. Although D_{8V} values are calculated to be 213–220 nm, as is comparatively depicted with D_{0V} in Figure 4b, the actual interparticle separations are larger as D denotes the center-to-center distance between the {111} layer.

To confirm the enhanced structural color and tunability of the CCA from PMMA–PtBMA core–shell μ -spheres, similarly sized PtBMA μ -spheres (200 nm) at similar μ -sphere and AOT concentrations (40 wt% and 130 mM) were prepared. The electrically tuned reflectance changes for both CCAs, up to 4 V bias, were plotted in Figure 5a,b. The inset schematic drawings demonstrate the PtBMA and core–shell μ -spheres, respectively, with the adsorbed AOT micelles.

Clearly, the absolute reflectance values are enhanced in the CCA from the core–shell μ -sphere because of the high-refractive-index PMMA core. Besides the increased reflectance values, the peaks from the core–shell μ -sphere CCA exhibit smaller full width at half maximum (FWHM) values under-voltage biases. This is another indication of improved colors. To compare electric tunability, the λ_{peak} versus voltage plots are compared in Figure 5c. For easier comparison, the λ_{peak} values were normalized to λ_{peak} at 0 V (λ_0 ; 638 vs 644 nm). As shown in Figure 5c,

the CCA of the core–shell μ -sphere showed $\lambda_{\text{peak}}/\lambda_0$ of 0.80 at 4 V (corresponding to 20% tunability), whereas that of the PMMA-only CCA was approximately 17% at 4 V. The better electric tunability of the CCA from core–shell μ -spheres is attributed to the higher surface charge that originates from the larger refractive index, as previously discussed.

Although an EPD with improved reflective colors and enhanced electric tunability was achieved by applying a PMMA–PtBMA μ -sphere, the Δn between the μ -sphere and the liquid medium still allowed a substantial light transmittance. This implies its applicability as a semi-transparent EPD. Figure 6a shows that the transmittance spectra were obtained from an EPD cell containing a 40 wt% CCA from 200-nm-sized PMMA–PtBMA μ -spheres between two ITO glasses. Without voltage bias, a strong attenuation of light transmission as low as 15% was observed at 620 nm due to the Bragg diffraction of light of $\lambda_{\text{peak}} = 620$ nm, whereas 40%–50% of light transmittances were observed upon voltage biases. Because of the non-zero transmittance of light through a display cell, a semi-transparent display was demonstrated and is shown in Figure 6b, where the photographs of the semi-transparent EPD cell were taken at different voltage biases. The background letters can be recognized through the color display as shown in Figure 6b, and they become clearer as the voltage increases. The transmittance is the lowest at 0 V (voltage OFF), and a higher transmittance is observed as the voltage increases, as shown in the spectra in Figure 6a. Reductions in both the reflectance and transmittance at the λ_{peak} with voltage bias are attributed to the decreasing crystallinity of the CCA and the appearance of the quasi-amorphous phase by electrophoretic movements of the μ -spheres.^[7a,j] A higher transmittance of the core–shell CCA with voltage bias is more evident in the movie clip (Supporting information).

Using the CCA of 40 wt% and the 190-nm-sized PMMA–PtBMA μ -spheres, time-dependent changes in the λ_{peak} during

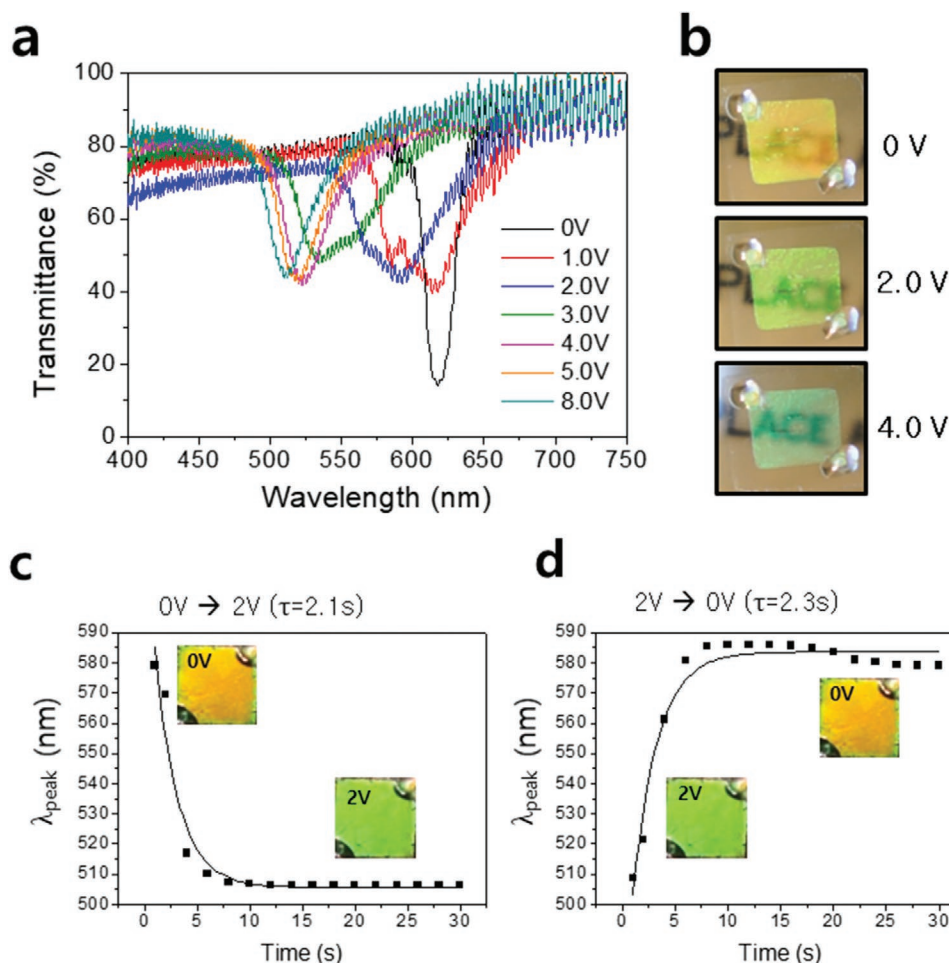


Figure 6. a) Transmittance spectra of a display cell (area = 1 cm²) containing a 40 wt.% CCA from 200-nm-sized PMMA–PtBMA μ -spheres with voltage biases from 0 to 8 V. b) Photographs showing the gauziness of the background letters through a semi-transparent color display at different voltage biases. Kinetic plots of λ_{peak} versus time upon changing voltage bias c) from 0 to 2 V and d) from 2 to 0 V on a display cell (area = 1 cm²) containing a 35 wt.% CCA from the 190-nm-sized PMMA–PtBMA μ -spheres. Single exponential function fit resulted in the response time for a blue shift of 2.1 s and a response time for a redshift of 2.3 s. Colors at each voltage are shown as inset photos in each plot.

voltage bias from 0 to 2 and 2 to 0 V were measured and plotted in Figure 6c,d. Both plots were fitted by exponential function to obtain the response time (τ) of approximately 2 s for both the blue-shifted and red-shifted color changes ($\tau_{0-2V} = 2.1$ s, $\tau_{2-0V} = 2.3$ s). A slow kinetics of E-driven color change of CCA in a non-polar medium can be attributed to the low dielectric constant of the medium as reported in the previous literature.^[71] Because of its smaller size, the 190-nm-sized PMMA–PtBMA μ -sphere produced an orange–yellow-colored CCA at 40 wt%, whereas the 200-nm-sized μ -sphere formed a red-colored CCA at the same solid content.

To examine the long-term stability as a reflective display, the 40 wt% CCA from the 190-nm-sized PMMA–PtBMA μ -spheres was subjected to repeated stepwise voltage biases of 0–2–4 V with a duration of 30 s at each voltage step. Figure 7a shows a plot of the λ_{peak} versus time during 50 cycles of repeated biases (= 150 voltage steps), where the reproducible λ_{peak} values are shown. The typical reflectance spectra and the reflective colors under halogen light illumination at each voltage step are shown in Figure 7b,c. The results confirmed that the reproducible full

RGB color changes were achieved using the core–shell EPD device without significant loss of color tunability or quality deterioration. Compared to the CCA from 200-nm-sized μ -spheres, $\Delta\lambda_{\text{peak}}$ between 0 and 4V appears to be significantly shorter in Figure 7, which can be attributed to a batch-to-batch deviation of μ -sphere property (Figure S4, Supporting Information). In addition, heterogeneous structural colors at different spots can be another source of deviation in λ_{peak} especially at 0V.

Upon 50 cycles of repeated voltage biases, an approximate 2% redshift in the λ_{peak} (483–492 nm) at the 4 V bias was observed, whereas less than a 1% shift was observed at 0 V. It is not clearly understood why a slight redshift in the λ_{peak} is observed at the 4 V voltage bias upon the repeated voltage cycles.

The low-angular dependency of the color display device is an essential prerequisite from a practical point of view. Using a homemade setup for angle-dependent reflectance measurement [as shown in Figure 8a], the reflectance spectra from an EPD cell were obtained with various angles from 0° to 40°. Figure 8b shows the angle-dependent reflectance spectra before voltage biasing, from which the λ_{peak} and percentage reflectance

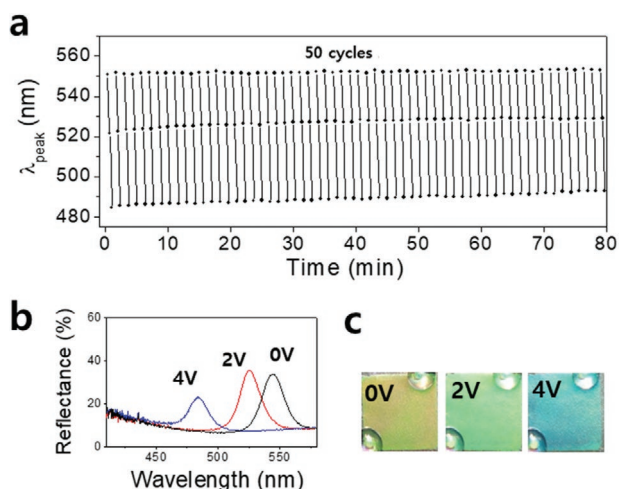


Figure 7. a) Plot of λ_{peak} versus time during 50 cycles of repeated biases where one voltage cycle corresponds to 0 V (30 s)–2 V (30 s)–4 V (30 s). The display cell (area = 1 cm²) contains a 40 wt.% CCA from the 190-nm-sized PMMA–PtBMA μ -spheres; 30 μ m Surlyn was used as a spacer. b) Reflectance spectra from a display cell at three different voltage steps of 0–2–4 V, and c) reflective colors of a display cell at each voltage, where orange (0 V), green (2 V), and blue (4 V) colors are reflected from halogen light illumination. Two holes (sealed with UV-curable resin) are shown in the photographs.

values were extracted and plotted in Figure 8c. Evidently, only a 3% change ($\Delta\lambda_{\text{peak}}/\lambda_{\text{peak}}$) in peak wavelength occurred. This small change implies a small angular dependency. Additionally, absolute reflectance values decreased significantly with angle variation. With the limited setup in this study, finding the same

angle variation spot was difficult; hence, precise measurements are not guaranteed. However, slight blue shifts and decreased color intensities were obvious with an increased viewing angle as shown in the inset photographs in Figure 8c. In another experiment, angle-dependent reflectance measurements were performed with voltage bias (Figure S6, Supporting Information), and the λ_{peak} versus voltage at four different angles were plotted in Figure 8d.

In this graph, the low-angle dependency of the core–shell EPD is reconfirmed. The low-angular dependency of the structural color implies that the colloidal arrays are predominantly quasi-amorphous structures rather than crystalline arrays. Figure 8d shows that the low-angular dependency was similar regardless of the voltage bias.

3. Conclusion

To achieve the improved structural colors and color tunability of the CCA-based full-color EPD in a non-polar medium, core–shell μ -spheres with 190–200 nm diameters were synthesized. These μ -spheres contained a high-refractive-index PMMA core and a PtBMA shell, ensuring a uniform colloidal dispersity in an isoparaffinic fluid. Introduction of AOT inverse micelles successfully developed the surface charges on the PMMA–PtBMA μ -spheres. These charges appeared as higher ζ values compared with those on the PtBMA μ -spheres within the given AOT concentration ranges. A higher surface charge was attributed to a stronger VDW interaction between the PMMA–PtBMA μ -sphere and the AOT inverse micelle (depending on the relative refractive index). Electric tuning of the

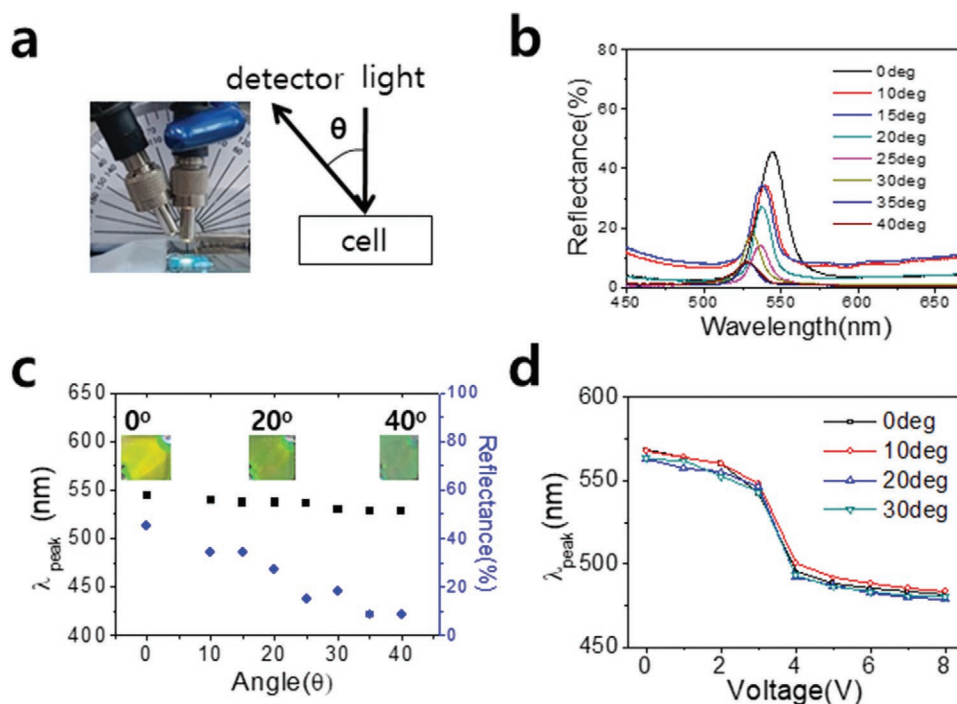


Figure 8. a) Apparatus for measurement of angle-dependent reflectance spectra, b) individual reflectance spectra with varying angles, and c) angular dependences of the λ_{peak} and percentage reflectance of a 35 wt.% CCA from the 190-nm-sized PMMA–PtBMA μ -spheres. The inset figures are the photographs taken at each angle. d) Plots of the λ_{peak} versus the voltage bias measured at four different angles.

the PMMA–PtBMA CCA clearly demonstrated enhanced reflectance values and smaller FWHMs of the diffraction peaks, as well as improved color tunability. The semi-transparent EPD, using the PMMA–PtBMA CCA, was demonstrated since the diffraction peaks showed 40% to 50% transmittance. The EPD showed a switching time of approximately 2 s for the color changes from orange to green and green to orange. The long-term stability of the PMMA–PtBMA EPD was examined by 50 voltage cycles of 0–2–4 V after which less than a 2% change in the λ_{peak} was observed. This finding implies that the EPD has good stability. Angle-dependent measurements of the reflectance spectra with voltage bias showed that the PMMA–PtBMA EPD has a low-angular dependency of structural colors. This is likely due to QACAs being the dominant structures in the presence of the electric field.

4. Experimental Section

Materials: Methylmethacrylate (MMA), t-Butylmethacrylate (tBMA), AOT (97%), ethylene glycol dimethacrylate (EGDMA), and potassium persulfate (KPS) were purchased from Sigma-Aldrich. Isopar G (IPG, Exxon Mobil, USA) and Halocarbon (HC, Halocarbon Co. Ltd., USA) were premixed before use. Aqueous dispersions of the as-synthesized μ -spheres were preserved in ion exchange resin (AG501-X8, Bio-Rad). Ethanol (99%) and 2-propanol (IPA, 99.5%) were purchased from Duksan. Surlyn (Meltonix 1170, 30 μm , SOLARONIX) was used as the spacer.

Preparation of the Microsphere Dispersion: PMMA–PtBMA core-shell μ -spheres were synthesized via surfactant-free emulsion polymerization;^[23] 250 mL of deionized (DI) water was charged in a reactor in a 500 mL three-neck round bottom flask and degassed via nitrogen bubbling for 30 min; 50 mg KPS and 25 mg KPS were dissolved in 2 mL aliquots of degassed DI water to prepare the first and second initiators, respectively. The temperature of the reactor was increased to 75 °C in an oil bath, where the first initiator was added. After nitrogen bubbling for 30 min, the mixture of MMA and EGDMA was rapidly added. After 1 h, a 10 mL aliquot was collected for the size analysis of the PMMA core, and one-fourth of the volume of tBMA to MMA from the second initiator was inserted. After 1 h, the milky suspension of PtBMA was filtered using cotton, centrifuged, and redispersed in DI water. Finally, a small amount of ion exchange resin was added in aqueous dispersion for the removal of trace amounts of impurities. The PtBMA μ -spheres were prepared through a similar procedure, only differing in the addition of a mixture of tBMA and EGDMA for core generation instead of a mixture of MMA and EGDMA. After centrifugation of the aqueous dispersion, the sedimented μ -spheres were redispersed in IPA and then centrifuged and redispersed again. Upon another centrifugation, the spheres were dispersed in an IPG/HC (1.71/1 by volume) mixture, which was premixed with AOT at various concentrations.

Characterizations: The refractive index of the liquid was measured using a digital refractometer (RX-5000, ATAGO), and conductivity was measured using a digital conductivity meter (model 1153, EMCEE Electronics, Inc.) The viscosity of liquid and the μ -sphere dispersion was measured using a viscometer (DV-II+ Pro, Brookfield). The zeta potential of the μ -sphere dispersion was measured using the Nicomp 380 ZLS (Particle Sizing Systems, Inc.). The CCA reflectance spectrum was measured using a reflected light microscope (L2003A, Birmence) through a 20X objective lens (NA = 0.3) coupled with a UV–vis spectrometer (AvaSpec, Avantes) with a halogen light source. Every spectrum was referenced by using a silver mirror (Edmund Optics).

Fabrication and Electric Tuning Performance Test of the Electrophoretic Display Cell: Two pieces of ethanol-washed indium tin oxide (ITO) glass (20 × 20 mm, 15–25 Ω , Wooyang GMS) were used as the top and bottom electrodes for the EPD cell. Two holes were drilled into the top ITO

glass through which the CCA dispersion was injected. Before the CCA introduction, a 30- μm -thick Surlyn film was cut to an open square shape (1 cm²) and attached between the ITO glasses by hot-pressing them at 70 °C. After the CCA infilling, the holes in the top ITO glass were sealed by a UV-curing resin (Secure, CP-7426, photopolymer) by exposing the resin to a UV lamp (Hoya Candeo Optronics Corp., EXECURE 4000-D) for 10 s (Figure S1, Supporting Information). An EPD cell was wired for voltage biasing to an automatic battery cyler (WBCS3000, WonATech), from which the anode was connected to the top ITO and the cathode was connected to the bottom ITO. The current was measured during voltage bias, and the reflectance spectra were collected using a UV–vis spectrometer (AvaSpec, Avantes) through a reflected light microscope. The photographs of electrically tuned color changes were collected using a digital camera (NEX-5N, SONY) with dual illumination from Hg fluorescent light and halogen light.

Supporting Information

Supporting Information is available from the Wiley Online Library or from the author.

Acknowledgements

W.L. appreciates Prof. Shin Hyun Kim and Hye Min Kim for helpful discussions. This study was financially supported by the Basic Science Research Program through the National Research Foundation of Korea (NRF), which was funded by the Ministry of Science, ICT, and Future Planning (Grant No. NRF-2019R1A2C1010088).

Conflict of Interest

The authors declare no conflict of interest.

Data Availability Statement

Research data are not shared.

Keywords

core–shell microspheres, crystalline colloidal arrays, electrophoretic displays, inverse micelles, non-polar medium

Received: April 25, 2021

Revised: July 18, 2021

Published online:

- [1] L. Nucara, F. Greco, V. J. Mattoli, *J. Mater. Chem. C* **2015**, *3*, 8449.
- [2] a) K. Ueno, K. Matsubar, M. Watanabe, Y. Takeoka, *Adv. Mater.* **2007**, *19*, 2807; b) D. P. Puzzo, A. C. Arsenault, I. Manner, G. A. Ozin, *Angew. Chem.* **2009**, *121*, 943; c) Y. Lu, H. Xia, G. Zhang, C. Wu, *J. Mater. Chem.* **2009**, *19*, 5952.
- [3] a) M. Ozaki, Y. Shimoda, M. Kasano, K. Yoshino, *Adv. Mater.* **2002**, *14*, 514; b) S. Kubo, Z. Z. Gu, K. Takahashi, A. Fujishima, H. Segawa, O. Sato, *J. Am. Chem. Soc.* **2005**, *126*, 8314.
- [4] M. Warner, E. M. Terentjev, *Liquid Crystal Elastomers*, Oxford University Press, Oxford, UK **2009**.
- [5] a) K. Ueno, J. Sakamoto, Y. Takeoka, M. Watanabe, *J. Mater. Chem.* **2009**, *19*, 4778; b) J. Xia, Y. Ying, S. H. Foulger, *Adv. Mater.* **2005**, *17*,

- 2463; c) Q. Zhao, A. Haines, D. Snoswell, C. Keplinger, R. Kaltseis, S. Bauer, I. Graz, R. Denk, P. Spahn, G. Hellmann, J. J. Baumberg, *Appl. Phys. Lett.* **2012**, *100*, 101902; d) J. Park, S. Yoon, N. Heo, W. Lee, *J. Ind. Eng. Chem.* **2020**, *88*, 117.
- [6] Y. Jiang, D. Xu, X. Li, C. Lin, W. Li, Q. An, C. Tao, H. Tang, G. Li, *J. Mater. Chem.* **2012**, *22*, 11943.
- [7] a) I. Lee, D. K. , J. Kal, H. Baek, D. Kwak, D. Go, E. Kim, C. Kang, J. Chung, Y. Jang, S. Ji, J. Joo, Y. Kang, *Adv. Mater.* **2010**, *22*, 4973; b) T. S. Shim, S. H. Kim, J. Y. Sim, J. M. Lim, S. M. Yang, *Adv. Mater.* **2010**, *22*, 4494; c) M. G. Han, C. G. Shin, S. J. Jeon, H. S. Shim, C. J. Heo, H. Jin, J. W. Kim, S. Y. Lee, *Adv. Mater.* **2012**, *24*, 6438; d) M. G. Han, C. J. Heo, C. G. Shin, H. S. Shim, J. W. Kim, Y. W. Jin, S. Y. Lee, *J. Mater. Chem. C* **2013**, *1*, 5791; e) Y. Luo, J. Zhang, A. Sun, C. Chu, S. Zhou, J. Guo, T. Chen, G. Xu, *J. Mater. Chem. C* **2014**, *2*, 1990; f) H. S. Shim, C. G. Shin, C. Heo, S. Jeon, H. Jin, J. W. Kim, Y. W. Jin, S. Y. Lee, J. Lim, M. G. Han, J. K. Lee, *Appl. Phys. Lett.* **2014**, *104*, 051104; g) M. Bellingeri, A. Chiasera, I. Kriegel, F. Scotognella, *Opt. Mater.* **2017**, *72*, 403; h) K. Chen, Q. Fu, S. Ye, J. Ge, *Adv. Funct. Mater.* **2017**, *27*, 1702825; i) Q. Fu, H. Zhu, J. Ge, *Adv. Funct. Mater.* **2018**, *28*, 1804628; j) K. H. Ko, E. Park, H. Lee, W. Lee, *ACS Appl. Mater. Interfaces* **2018**, *10*, 11776; k) W. Wang, A. Zheng, Y. J. , D. Lan, F. Lu, L. Zheng, L. Zhuang, R. Hong, *RSC Adv.* **2019**, *9*, 498.
- [8] a) J. Jacobson, B. Comiskey (Mass. Inst. Technology), US Patent US 5930026, **1996**; b) Einkgroup.com, E Ink Holdings – About us, www.einkgroup.com (accessed: March 2021).
- [9] M. F. Hsu, E. R. Dufresne, D. A. Weitz, *Langmuir* **2005**, *21*, 4881.
- [10] J. Ge, L. He, J. Goebel, Y. Yin, *J. Amer. Chem. Soc.* **2009**, *131*, 3484.
- [11] G. S. Roberts, R. Sanchez, R. Kemp, T. Wood, P. Bartlett, *Langmuir* **2008**, *24*, 6530.
- [12] M. Kotlarchyk, J. S. Huang, S. J. Chen, *J. Phys. Chem.* **1985**, *89*, 4382.
- [13] J. H. Park, M. A. Lee, Y. H. Kim, B. J. Park, H. Choi, *J. Korean Phys. Soc.* **2008**, *53*, 50.
- [14] H. Cao, Y. Cheng, P. Huang, M. Qi, *Nanotechnology* **2011**, *22*, 445709.
- [15] P. G. Smith, M. N. Patel, J. W. Kim, T. E. Milner, K. P. Johnston, *J. Phys. Chem. C* **2007**, *111*, 840.
- [16] B. V. Derjaguin, L. Landau, *Acta Physicochim. URSS* **1941**, *14*, 633.
- [17] C. Randall, J. V. Tassel, in *Encyclopedia of Materials: Science and Technology* (Ed: K. H. J. Buschow), Elsevier, Amsterdam, Netherlands **2001**.
- [18] F. Beunis, F. Strubbe, M. Karvar, O. Drobchak, T. Brans, K. Neyts, A. R. M. Verschueren, *Colloids Surf., A* **2014**, *440*, 10.
- [19] F. Beunis, F. Strubbe, K. Neyts, A. R. M. Verschueren, *Appl. Phys. Lett.* **2007**, *90*, 182103.
- [20] S. C. Gil, Y. G. Seo, S. Kim, J. Shin, W. Lee, *Thin Solid Films* **2010**, *518*, 5731.
- [21] G. N. Smith, J. Eastoe, *Phys. Chem. Chem. Phys.* **2013**, *15*, 424.
- [22] S. K. Sinis, V. Germain, C. O. Mejean, E. R. Dufresne, *Langmuir* **2008**, *24*, 1160.
- [23] S. Kim, Y. G. Seo, Y. Cho, J. Shin, S. C. Gil, W. Lee, *Bull. Korean Chem. Soc.* **2010**, *31*, 1891.